CFD ANALYSIS OF EFFECT OF VISCOSITY AND RPM

ON AN ELECTRICAL SUBMERSIBLE PUMP

A Thesis

by

RAHUL AGARWAL

Submitted to the Office of Graduate and Professional Studies of
Texas A&M University
in partial fulfillment of the requirements for the degree of

MASTER OF SCIENCE

Chair of Committee,	Gerald Lee Morrison
Committee Members,	Michael Pate
	Karen Vierow Kirkland
Head of Department,	Andreas A. Polycarpou

May 2017

Major Subject: Mechanical Engineering

ABSTRACT

Computational fluid dynamics analysis (CFD) has been employed to study the flow behavior, and dependency of pump efficiency and head on the operating conditions of the pump and fluids pumped. Commercially available ANSYS Fluent is the tool used in this study for simulation of flow through the pump. A single stage of an ESP (Electrical submersible pump) WJE-1000, manufactured by Baker Hughes Ltd., is modeled and investigated. A three dimensional single phase flow has been considered for the numerical simulations to study pump performance, over a range of flow rates, viscosities and rotational speeds.

It is shown that the pump speed does not affect the head coefficient and efficiency when plotted against flow coefficient, or in a more general sense, dimensionless parameters, when plotted against each other, are not affected by a change in rpm. Also, efficiency for all the cases can be represented on a single curve which includes flow coefficient and rotating Reynold's number. It is also shown that careful selection of the CFD model is indeed very important and more work needs to be done in that regard.

The ramifications of these results are very significant. The affinity laws have been modified to include the effects of viscosity. Hence a single head coefficient curve and a single efficiency curve (power required to operate the pump) can represent the pump performance over the entire flow rate and pump speed envelop. This will allow operators to be able to predict changes in pump performance with varying fluids and pump speeds.

An additional benefit is that a pump need not be tested over a wide range of fluids, but only at two viscosities in order to obtain power law coefficient on Re_w. Once the relationship has been determined for a specific pump design, it can be published and utilized for all operating conditions.

ACKNOWLEDGEMENTS

I would like to thank my committee chair, Prof. Gerald Morrison, and my committee members, Dr. Pate and Dr. Vierow, for their guidance and support throughout the course of this research.

Thanks to Dr. Abhay Patil for his invaluable help, guidance and support throughout the course of my research.

Thanks to Jeff Shive for his help and support that made my research a lot more comfortable.

Thanks also go to my friends and colleagues and the department faculty and staff of Texas A&M University.

Finally, I would like to express my gratitude to my entire family for making this endeavor possible.

CONTRIBUTORS AND FUNDING SOURCES

Contributors Section

Part 1, faculty committee recognition

This work was supervised by a thesis committee consisting of Dr. Gerald Morrison of the Department of mechanical Engineering, Dr. Michael Pate of the Department of mechanical Engineering, and Dr. Karen Kirkland of the Department of Nuclear Engineering.

Part 2, student/collaborator contributions

All work for the thesis was completed independently by the student.

Funding Section

Graduate study was supported by graduate teaching assistantships from Texas A&M University.

NOMENCLATURE

ESP	Electrical Submersible Pump
BEP	Best Efficiency Point
D_h	Hydraulic diameter
A_{in}	Inlet cross section area
D_s	Length scale for pump geometries
Q	Volumetric flow rate
ΔP	Pressure difference
H	Head
T	Torque on the shaft
$\mathscr{P}_{sh}$	Shaft power
$\mathscr{P}_{drag}$	Drag power
N_{sh}	Shaft power coefficient
N_{out}	Output power coefficient
N_{drag}	Drag power coefficient
Re_{Dh}	Reynold number based on hydraulic diameter
Re_w	Rotating Reynolds number
g	Acceleration due to gravity
gpm	Gallons per minute
rpm	Revolutions per minute
h	Blade Height

t	Blade thickness
ρ	Density of fluid
μ	Dynamic viscosity of fluid
ν	Kinematic viscosity of fluid
ω	Angular speed of pump
η	Pump efficiency
Φ	Flow rate coefficient
Ψ	Head coefficient

Subscripts

1	Impeller inlet
2	Impeller outlet
3	Diffuser inlet
4	Diffuser outlet

TABLE OF CONTENTS

LIST OF FIGURES

LIST OF TABLES

1. INTRODUCTION

The focus of this study is the electrical submersible pump, as used mainly in pumping/lifting oil from low pressure reservoirs to increase the flow out of the reservoir. Artificial lift is a means of overcoming low bottom-hole pressure to produce oil from the well at a pre-determined desired rate.

Artificial lift as a method of production, is generally associated with mature, depleted fields, where the natural pressure has declined such that the reservoir can no longer produce under its natural energy. However, it can also be used in younger fields to increase the production rate. Artificial lift methods can be broadly categorized in the following categories: electrical submersible pump, rod sucker pump, gas lift, plunger lift, progressive cavity pump and hydraulic pump.

An ESP (electrical submersible pump) is a type of dynamic displacement pump, which moves the fluid from inlet to outlet under its own momentum, i.e. it transfers its momentum to the fluid. The electrical energy is transferred through the rotating blades of the centrifugal ESP to the fluid that is passing through it, which therefore, increases the pressure of the fluid at the discharge. The pump is positioned vertically inside the well bore. It generally consists of multiple stages or stacks of impellers and diffusers (an impeller and diffuser forms a stage). The impeller is connected to a rotating shaft (source of energy input) which transfers the energy to the fluid, which then passes through the stationary diffuser. This completes a single stage. The exit of this diffuser acts as the inlet to the next stage impeller and so on. The pressure difference between the inlet and exit of the pump is the head generated by that pump and represents the total amount of energy

gained by the fluid as a result of the pumping action. The downhole centrifugal pump is connected to a power source at the surface, Fig. I-1.

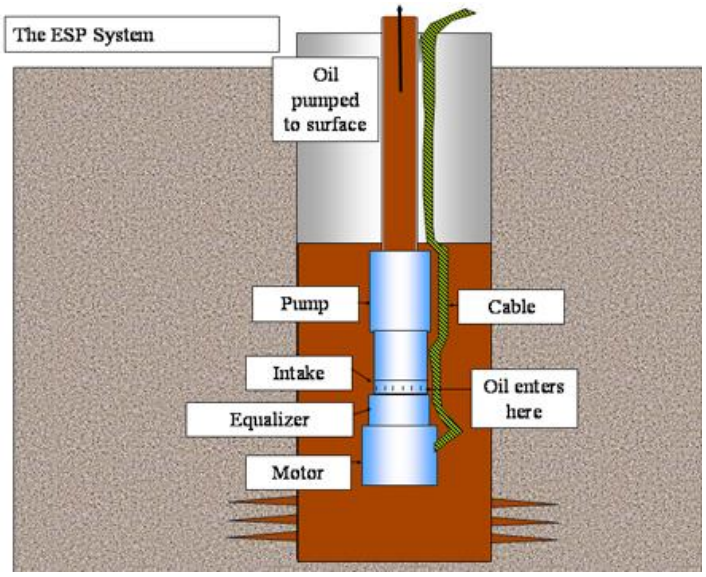

Figure I-1. Representative view of an ESP.

The important input parameters for a pump are the flow rate of the fluid, rotational speed of the shaft, the fluid properties such as density and viscosity and the operating environment i.e. temperature. Therefore, it is important to have an understanding of the pump behavior, most importantly the output parameters which can be quantified in terms of head generated by the pump and the hydraulic efficiency of the pump.

2. LITERATURE REVIEW

The fundamental concepts of centrifugal pumps were introduced by Karassik [1]. He discussed the detailed structure, construction, performance, selection and development of centrifugal pumps. The performance is characterized by head, conditions of service and specific speed. For selection of the pump, the most important criterion was deemed to be desired capacity and the head against which the pump is to be used.

Ippen [2] conducted extensive experiments to study the effect of viscosity and specific speed on 4 different pumps which were single stage single suction pump with closed type impellers (IL11), single stage single suction pump with open type impellers (IL12), single stage double suction pump with impeller diameter 69/8 inch (IL21) and single stage double suction pump with impeller diameter 83/16 inch (IL22). He concluded that performance was affected by major losses which could be categorized into three zones based on Reynold's number $R_D = \frac{\omega r_2^2}{\nu}$. For $R_D > 10^6$ efficiency losses were mainly due to hydraulic through flow losses. For $10^6 > R_D > 10^4$, disk and ring friction losses were the main contributor to an increase in power input. For $R_D < 10^4$, through flow losses assumed the dominant role. However, this study was not applicable to pumps across the spectrum.

Gulich [3], [4] studied pumping of highly viscous fluids with centrifugal pumps and provided a detailed analysis of losses in case of viscous fluids which involved greater complexities as compared to service with water. He defined the efficiency factor f_η as

$f_\eta = f_H \frac{1+\left(\frac{P_{RR}}{P_u}\right)_w f_{RS}\eta_{vol}\eta_{h,w}}{1+\left(\frac{P_{RR}}{P_u}\right)_w \frac{f_{RS}k_{RR,v}f_{therm}}{f_Q k_{RR,w}}\eta_{vol}\eta_{h,w}}$ and concluded that this factor applied at BEP and other flow rates as well.

Timar [5] performed a dimensionless study involving flow coefficient, head coefficient and efficiency. The results are depicted in the following figures:

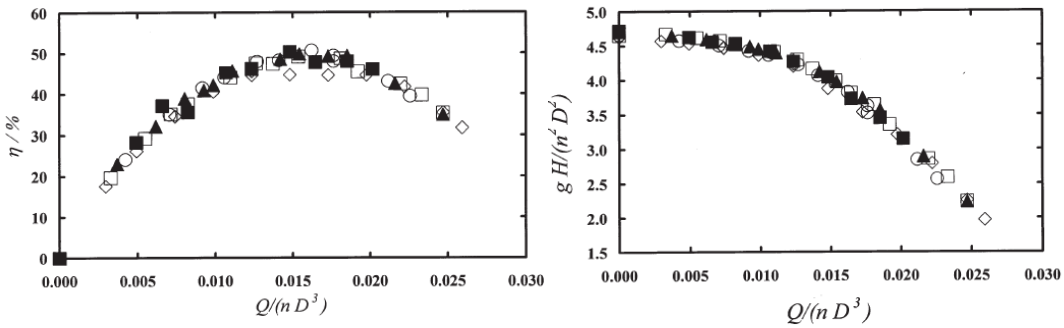

Figure II-1 Variation of efficiency (%) (left), and head coefficient (right) with flow coefficient for centrifugal pump. ◇ 2000 min^{-1}, Re = 681800; □1800 min^{-1}, Re = 613600; ▲1600 min^{-1}, Re = 545500; ○ 1400 min^{-1}, Re = 477300; ■ 1200 min^{-1}, Re = 409100 [5].

He (Fig. II-1) concluded that a dimensionless number π_{LIQUID} defined as the product of Reynold's number and flow coefficient was suitable to estimate the pump characteristics across the fluids, as the important idea is that this dimensionless number includes the liquid properties viz. viscosity and density and the flow rate of the liquid and rotational speed thereby covering all the input conditions. Therefore one could use the same numbers and trend to predict the behavior for a new liquid.

Feng [6] (Fig. II-2) used Ansys CFX-11 to solve Navier Stokes equations employing different turbulence models and concluded that for pressure difference calculations, the choice of model did not have a major bearing on the results

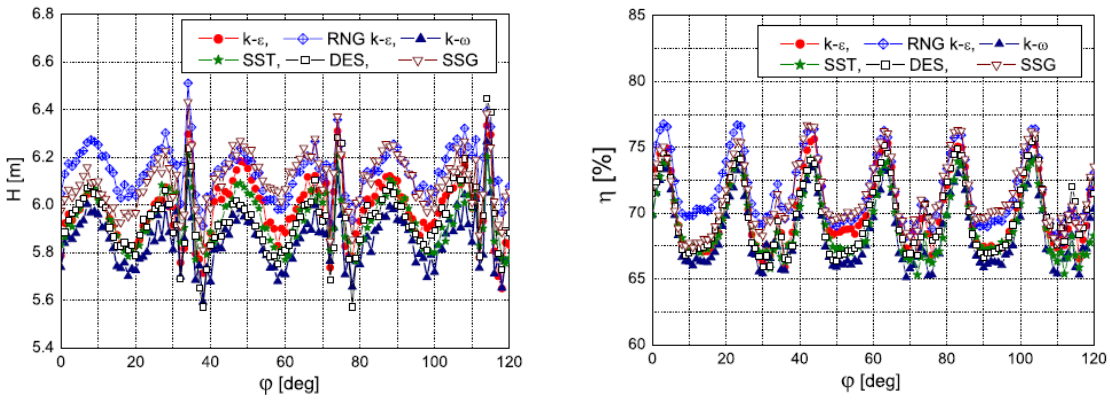

(a) Head (b) Hydraulic efficiency

Figure II-2 Figures (a) and (b) show the head and efficiency respectively for different impeller positions employing different turbulence models. [6].

Majidi [7] used standard $k-\epsilon$ turbulence model to simulate 3-D viscous flow inside a pump volute. He analyzed the characteristics of the secondary flow which in turn verified the reliability of the CFD study.

Barrios [8] studied both single phase flow and 2-phase flow inside an ESP with good agreement between the CFD and experimental results.

Sun [9] (Fig. II-3) proposed new models for pump frictional and shock losses for an ESP. He also showed good agreement between the head as predicted by the simulation model and that predicted by the affinity laws.

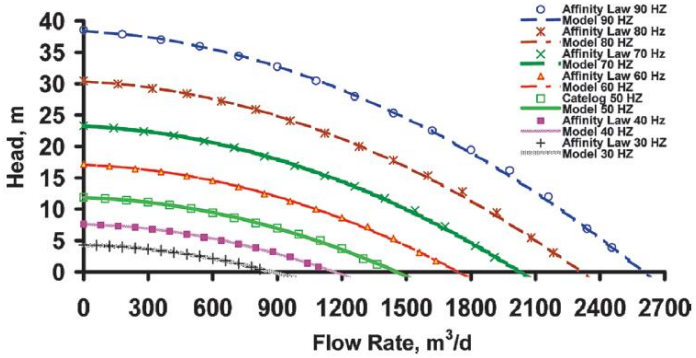

Figure II-3 Pump performance for different rotational speeds for water. [9].

Sirino [10] (Fig. II-4) studied the influence of viscosity on the performance of an ESP. He concluded that similarity held very well for low viscosities with changing rotational speeds, whereas specific head was degraded as the rotor speed decreased for a high viscosity fluid.

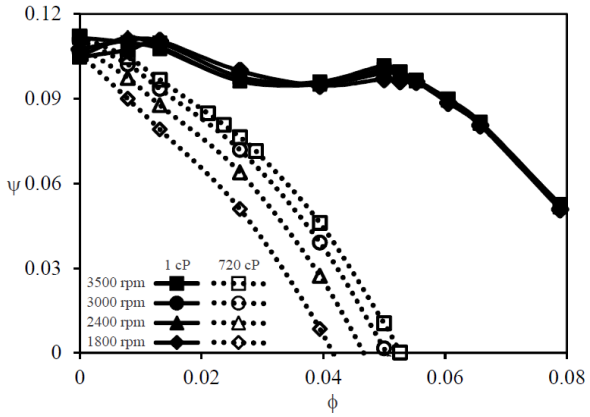

Figure II-4 Comparison of specific head (head coefficient) versus specific capacity (flow coefficient) between water and a 720 *cP* fluid, at four different rotor speeds. [10].

Stel [11] (Fig. II-5) investigated the effect of viscosity on a three stage ESP and found a better agreement between experimental and CFD results as compared to his previous simulations on a single stage ESP considering the same pump. He also concluded that head and hydraulic efficiency curves for operation with a range of viscosities and rotation speeds but same Reynolds numbers matched perfectly.

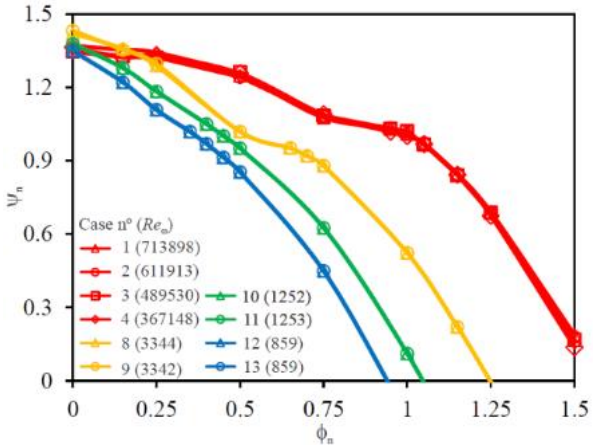

Figure II-5 Normalized head coefficient versus normalized flow coefficient, for matching Reynold's numbers. [11].

Yin [12] (Fig. II-6) performed a CFD study of the influence of viscosity (1 cP - 400 cP) on an ESP (WJE-1000) and showed that the head performance information could be represented in the form of non-dimensional numbers viz. head coefficient ψ, flow coefficient ϕ, and Reynold's number Re_w on a plot of ψ vs $\phi * Re_w^{-0.066}$, which is shown below for a single pump speed.

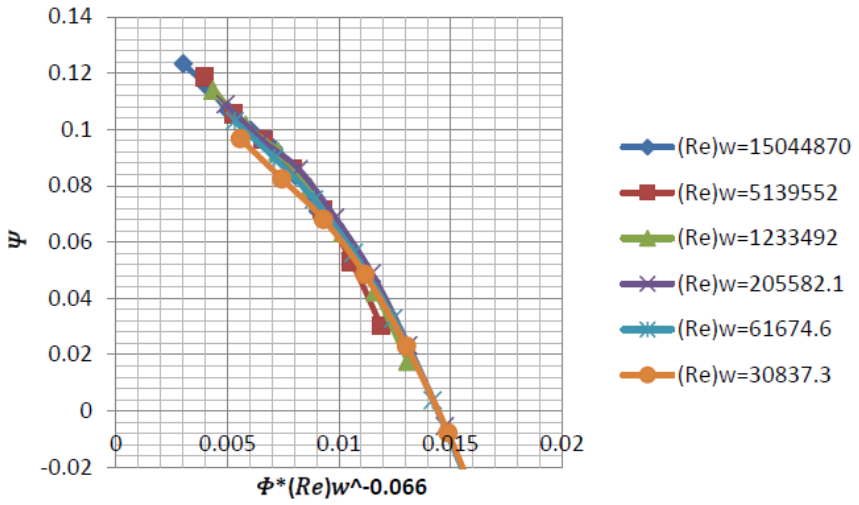

Figure II-6 Empirical pump performance curve. [12].

3. OBJECTIVE

In pumping crude oil, pump performance generally depends on viscosity, rotational speed of the pump, flow rate through the pump and pump geometry. In order to have a better understanding of the effect of variation of the above listed parameters on the head and efficiency of an ESP, a CFD analysis has been performed using ANSYS Fluent software [13].

For simplicity, a single stage has been considered, i.e. to have an understanding of the concept itself, a single stage was deemed sufficient. The geometry considered has been reasonably simplified by neglecting the balance holes (Fig. IV-6, IV-7, IV-8). The pump under consideration is the WJE-1000, manufactured by Baker Hughes Ltd. Meshing of the pump geometry has been done using Gambit. Fluent has been used for the simulation and post processing of results include the usage of Tecplot [14] and CFD Post as well.

Transient, single phase flow has been considered in this work. This is the same setup used by Yin [12] .This work adopts the same setup (which was already validated with experimental results by Yin [12]), and studies the effect of variation of rpm of the pump on its head and efficiency.

The head coefficient has been considered to study the head generated by the pump, as affected by viscosity, flow rate and rpm (quantified by the rotating Reynold's number), and efficiency has been considered to study the overall performance of WJE-1000.

4. MODELING PROCEDURE

4.1. Pump

Centrilift WJE-100 pump, manufactured by Baker Hughes is the ESP under consideration. It is a multiple stage centrifugal pump. The mixed flow type impeller has 5 blades and 5 balance holes(Fig. IV-1, IV-2). Diffuser has 7 vanes (Fig. IV-3, IV-4).

Figure IV-1 Impeller (WJE-1000). [15].

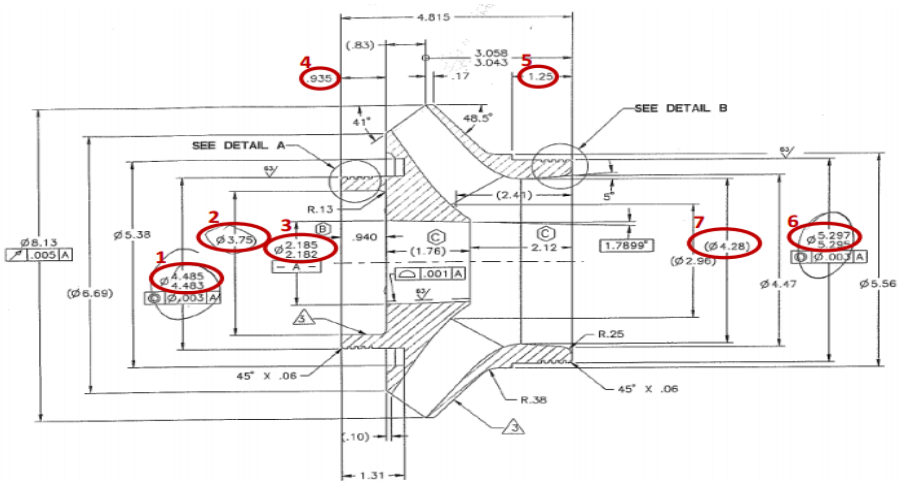

Figure IV-2 Dimensions of impeller of WJE-1000. [15], listed in Table IV-1.

Table IV-1 Dimensions of impeller and diffuser. The variables have meanings as defined earlier (in the nomenclature).

(mm)	Impeller	Diffuser
Blades/Vanes	5 blades	7 vanes
Inlet inner diameter	$D_{1,i} = 48.2$	$D_{3,I} = 183.0$
Inlet outer diameter	$D_{1,o} = 116.5$	$D_{3,o} = 218.6$
Inlet blade height	$h_1 = 35.0$	$h_3 = 19.8$
Inlet blade thickness	$t_1 = 4.8$	$t_3 = 3.8$
Outlet inner diameter	$D_{2,i} = 183.0$	$D_{4,i} = 48.2$
Outlet outer diameter	$D_{2,o} = 218.6$	$D_{4,o} = 116.5$
Outlet blade height	$h_2 = 24.8$	$h_4 = 22.9$
Outlet blade thickness	$t_2 = 2.1$	$t_4 = 4.8$

Figure IV-3 Discharge view of diffuser. It has seven vanes.

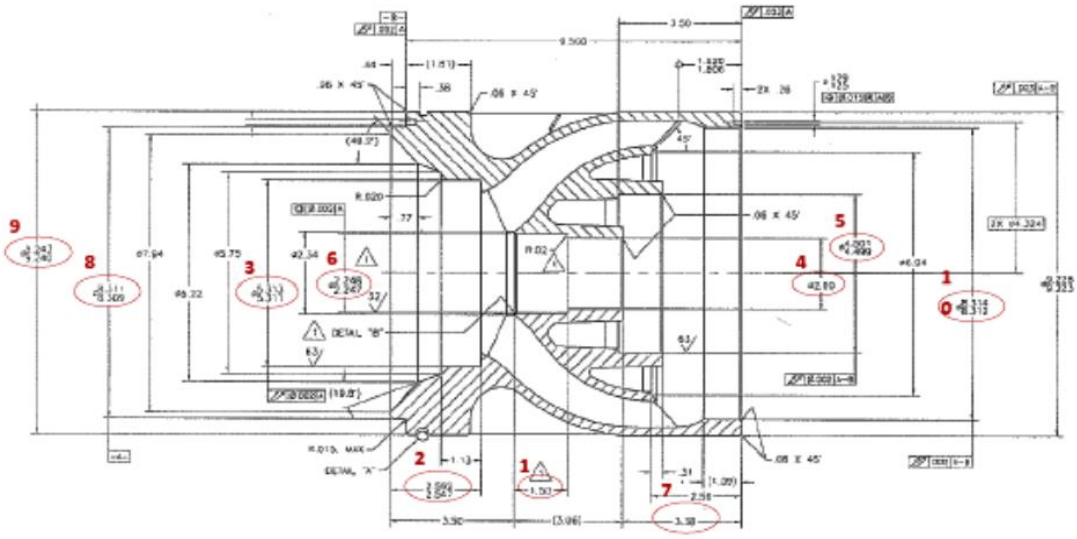

Figure IV-4 Dimensions of diffuser. [15]. These are also listed in Table IV-1**.**

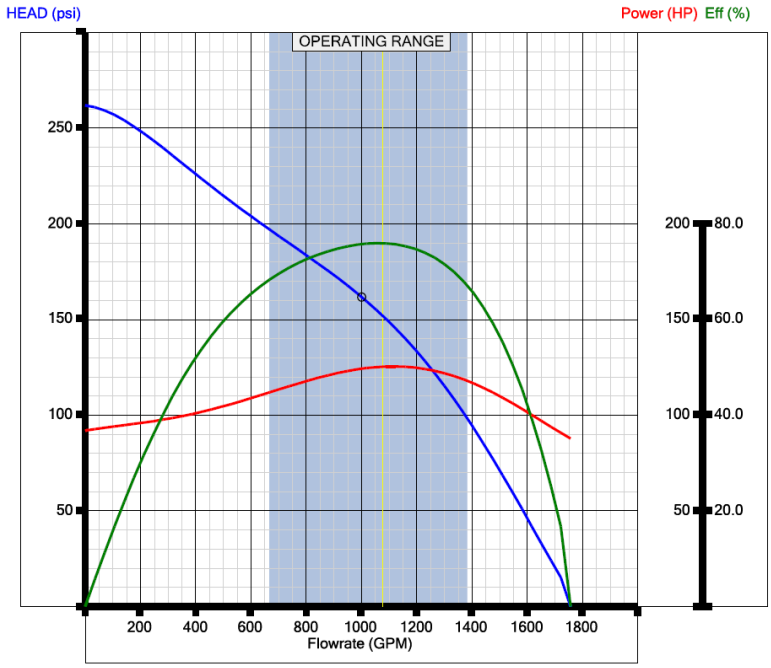

Figure IV-5 Catalogue performance curve of three stage WJE-1000 at 3600 rpm. [15].

It delivers a flow rate of approximately 1100 gpm with a pressure rise of 150 psi at the best efficiency point of 3600 rpm for three stages (Fig. IV-5).

4.2 Model and Mesh

The CAD model of single stage impeller and diffuser is shown in the figure below.

Figure IV-6 CAD model of impeller (left) and diffuser (right) of a single stage of ESP WJE 1000. [12].

Figure IV-7 Simplified CAD model of impeller (Balance holes neglected) (left) and diffuser (right). [12].

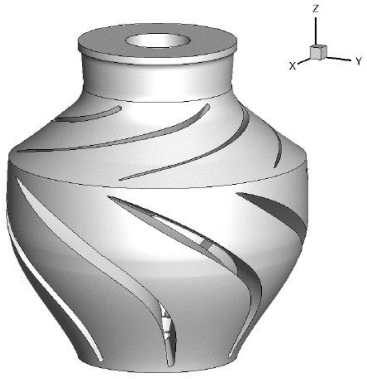

Figure IV-8 Final model of single stage of WJE-1000. [12]. Secondary flow paths and seal leakages have not been included. The inlet is at the top and discharge at the bottom.

The direction of flow at the inlet is specified to be normal to the inlet face. Since, pressure difference is the quantity of interest, therefore, a fixed reference value of pressure is assigned at the discharge of the pump (diffuser) for ease of calculations. No slip boundary condition has been imposed at all the surfaces. All the clearances and the gaps have been ignored and only the primary pump flow paths are considered. Using Gambit, meshing was done with hexahedral elements. To increase the accuracy, blades and edges have denser meshes as compared to the rest of the geometry. ANSYS Fluent [13] imports this mesh for numerical simulations.

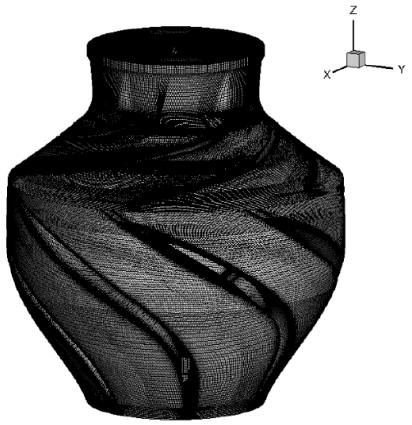

Figure IV-9 Mesh of single stage of WJE-1000 (simplified model).

A grid independence study was performed by Yin [12] to conclude that an increase in the number of nodes from 6,763,011 to 8,609,436 leads to a marginal increment in pressure rise across the stage of 0.07%. Therefore, the original mesh with 6,763,011 nodes was adopted for the analysis (Fig. IV-9).

5. SIMULATION SETUP

5.1. Reynold's Number

In this work, Stel's [11] definition of Reynold's number has been used to classify the flow regimes with respect to turbulence.

$$Re_{\mathrm{Dh}} = \frac{\left(\frac{Q}{A_{in}}\right).D_h.\rho}{\mu}$$

Where, the variables as previously defined, are flow rate, inlet cross section area, hydraulic diameter at the inlet, density of the fluid, and dynamics viscosity of the fluid. Hydraulic diameter is given as : $D_h = D_{1,o} - D_{1,i}$ i.e. the difference between impeller outlet and inlet diameters.

Although the dependence of flow nature on Reynold's number is rather vague, still, for the sake of categorization, the cases with Re_{Dh} less than 2300 were treated to be laminar whereas those with Re_{Dh} greater than 2300 were considered as turbulent [11].

5.2. Governing Equations

The standard $k-\epsilon$ model has been used for the turbulent flow cases. The numerical model used in Fluent [13] is based on Reynold's Averaged Navier Stokes Equations (RANS). $'k'$ stands for turbulent kinetic energy and $'\epsilon'$ stands for dissipation rate. The set of equations are given below:

$$\frac{\partial}{\partial t}(\rho k) + \frac{\partial}{\partial x_i}(pku_i) = \frac{\partial}{\partial x_j}\left[\left(\mu + \frac{\mu_t}{\sigma_k}\right)\frac{\partial k}{\partial x_j}\right] + G_k + G_b - \rho\epsilon - Y_M + S_k \qquad \text{(V-1)}$$

$$\frac{\partial}{\partial t}(\rho\epsilon) + \frac{\partial}{\partial x_i}(\rho\epsilon u_i) = \frac{\partial}{\partial x_j}\left[\left(\mu + \frac{\mu_t}{\sigma_\epsilon}\right)\frac{\partial \epsilon}{\partial x_j}\right] + C_{1\epsilon}\frac{\epsilon}{k}(G_k + C_{3\epsilon}G_b) - C_{2\epsilon}\rho\frac{\epsilon^2}{k} + S_\epsilon \quad \text{(V-2)}$$

$$G_k = -\rho\overline{u_i' u_j'}\frac{\partial u_j}{\partial x_i} \quad \text{(V-3)}$$

$$G_k = \mu_t S^2 \quad \text{(V-4)}$$

$$S = \sqrt{2S_{ij}S_{ij}} \quad \text{(V-5)}$$

$$G_b = -g_i\beta\frac{\mu_t}{Pr_t}\frac{\partial T}{\partial x_i} \quad \text{(V-6)}$$

$$Y_M = 0 \quad \text{(V-7)}$$

$$\mu_t = \rho C_\mu \frac{k^2}{\epsilon} \quad \text{(V-8)}$$

$$\beta = -\frac{1}{\rho}\left(\frac{\partial \rho}{\partial T}\right)_p \quad \text{(V-9)}$$

G_k is the turbulence kinetic energy generated by the mean velocity gradient, which can be modified to (V-4) under Boussinesq's assumption. G_b is the turbulence kinetic energy generated by buoyancy. P_{rt} is the Prandtl number for turbulence energy, g_i is the component of gravity, β is the coefficient of thermal expansion. Y_M is the dissipation due to compressible turbulence which has been neglected. σ_k is the turbulent Prandtl number for k equation (V-1), whereas σ_ϵ is the turbulent Prandtl number for ϵ equation (V-2). S_k and S_ϵ are the user defined source terms. The model constants are set to Fluent default settings and are given as:

$$C_\mu = 0.09 \tag{V-10}$$

$$C_{1\epsilon} = 1.44 \tag{V-11}$$

$$C_{2\epsilon} = 1.92 \tag{V-12}$$

$$C_{3\epsilon} = 1.3 \tag{V-13}$$

$$\sigma_k = 1.0 \tag{V-14}$$

$$\sigma_\epsilon = 1.3 \tag{V-15}$$

Standard wall functions based on Launder and Spalding's assumptions have been used in the simulations. The mean velocity U^* is given as:

$$U^* = \frac{1}{k}\ln(Ey^*) \tag{V-16}$$

$$U^* = \frac{\rho U_p C_\mu^{0.25} k_P^{0.5}}{\tau_\omega} \tag{V-17}$$

$$y^* = \frac{\rho C_\mu^{0.25} k_P^{0.5} y_P}{\mu} \tag{V-18}$$

where, $k = 0.42$ is the von Karman constant. $E = 9.81$ is the empirical constant, U_P is the mean velocity of particle at point P, k_P is the turbulence kinetic energy at point P.

For the laminar flow cases, Fluent solves the unsteady Navier Stokes equations, whose incompressible non-dimensional form is:

$$\frac{\partial \rho}{\partial t} + \nabla \cdot \rho \boldsymbol{v}_r = 0 \tag{V-19}$$

$$\frac{\partial}{\partial t}\rho \boldsymbol{v} + \nabla \cdot (\rho \boldsymbol{v}_r \boldsymbol{v}) + \rho(\boldsymbol{w} \times \boldsymbol{v}) = -\nabla p + \nabla \tau + \boldsymbol{F} \tag{V-20}$$

$$\frac{\partial}{\partial t}\rho E + \nabla \cdot (\rho \boldsymbol{v}_r H + \rho \boldsymbol{u}_r) = \nabla \cdot (k \nabla T + \tau \cdot \boldsymbol{v}) + S_h \tag{V-21}$$

Equations V-19, V-20, V-21 represent mass, momentum and energy conservation respectively.

5.3. Test Fluids

The following tables (V-1, V-2, V-3) provide the details of various cases that has been considered in this work. The test fluid for all the cases is C-200 (Conosol) [16] oil with density 818.4 kg/m^3.

Table V-1. Operating conditions for 2.4cP cases.

Viscosity (cP)	RPM	Flow Rate (gpm)	Re_w	Re_{Dh}
2.4	3000	444.7	4319482	73943.140
2.4	3000	741.06	4319482	123219.385
2.4	3000	1037.63	4319482	172531.488
2.4	3000	1334.09	4319482	221826.199
2.4	3600	533.64	5183378.4	88731.768
2.4	3600	889.27	5183378.4	147863.262
2.4	3600	1245.15	5183378.4	207037.785
2.4	3600	1600.91	5183378.4	266191.438
2.4	4200	622.58	6047274.8	103520.396
2.4	4200	1037.48	6047274.8	172507.139
2.4	4200	1452.68	6047274.8	241544.083
2.4	4200	1867.73	6047274.8	310556.678

Table V-2. Operating conditions for 60cP cases.

Viscosity (cP)	RPM	Flow Rate (gpm)	Re_w	Re_{Dh}
60	3000	444.7	172779.28	2957.726
60	3000	741.06	172779.28	4928.775
60	3000	1037.63	172779.28	6901.260
60	3000	1334.09	172779.28	8873.048
60	3600	533.64	207335.136	3549.271
60	3600	889.27	207335.136	5914.530
60	3600	1245.15	207335.136	8281.511
60	3600	1600.91	207335.136	10647.658
60	4200	622.58	241890.992	4140.816
60	4200	1037.48	241890.992	6900.286
60	4200	1452.68	241890.992	9661.763
60	4200	1867.73	241890.992	12422.267

Table V-3. Operating conditions for 400cP cases.

Viscosity (cP)	RPM	Flow Rate (gpm)	Re_w	Re_{Dh}
400	3000	444.7	25916.892	443.659
400	3000	741.06	25916.892	739.316
400	3000	1037.63	25916.892	1035.189

Table V-3 Continued

Viscosity (cP)	RPM	Flow Rate (gpm)	Re_w	Re_{Dh}
400	3000	1334.09	25916.892	1330.957
400	3600	533.64	31100.2704	532.391
400	3600	889.27	31100.2704	887.180
400	3600	1245.15	31100.2704	1242.227
400	3600	1600.91	31100.2704	1597.149
400	4200	622.58	36283.64881	621.122
400	4200	1037.48	36283.64881	1035.043
400	4200	1452.68	36283.64881	1449.264
400	4200	1867.73	36283.64881	1863.340

The density of oil C-200 has been obtained from the manufacturer [16]. For the sake of computational efficiency and to focus the attention on effects of rpm and viscosity itself, the energy equation has not been solved, therefore the dependence of viscosity and density on temperature has not been considered. Two definitions of Reynold's numbers have been used in this study. Rotational Reynold's number $Re_w = \frac{\rho \omega^2 D_s}{\mu}$ where, ρ is the density of fluid in kg/m^3 , ω is the rotational speed of the pump in rad/s , $D_s = 200.8\, mm$ is the length scale of pump geometries, impeller outlet mean diameter in this study, μ is the dynamic viscosity of fluid under consideration in $kgm^{-1}s^{-1}$. The Reynold's number or the actual Reynold's number or the hydraulic Reynold's number is defined as:

$$Re_{Dh} = \frac{\rho\left(\frac{Q}{A_{in}}\right)D_h}{\mu} \tag{V-22}$$

where, ρ is the density in kg/m^3, Q is the flow rate in m^3/s, $A_{in} = 0.00885\ m^2$, is the inlet cross section area of WJE-1000, $D_h = 68.4\ mm$ is the hydraulic diameter which equals the difference between impeller inlet inner and outer diameters. For the cases with, $Re_{Dh} < 2300$, laminar model has been utilized in Fluent, whereas for the cases with $Re_{Dh} > 2300$, standard $k - \epsilon$ turbulent model has been used.

5.4. Boundary Conditions

The choice of the time step size (transient simulations) has been made based on Yin's work [12]. Time step size in this study is $4.62963 \times 10^{-5}s$, and the total number of time steps considered are 798. To maintain consistency with respect to boundary conditions, the same time step was used in all the cases.

A fixed inlet flow rate was specified for each of the cases along with the rpm, viscosity and density of the fluid to completely specify the operating conditions. A fixed reference pressure of 100 psi was imposed at the outlet, which does not affect the results of simulations in any way, it could be set to any value, all it does is to change the inlet pressure in order to maintain the actual head or pressure rise of the pump. Initial guess value for inlet pressure was taken as zero psi, which again does not make any difference.

The inner walls of the impeller and inlet were considered rotational and the no slip condition was enforced at the walls. The diffuser has been considered as stationary with no slip.

6. RESULTS AND DISCUSSION

6.1. Pump Performance

The most important function of the pump in our study is the pressure rise it can generate under a particular set of operating conditions and environment. This important quantification of the pump performance is classically represented by the non-dimensional head coefficient and efficiency as a function of flow coefficient. These relationships are called the affinity laws and will be used to represent the results.

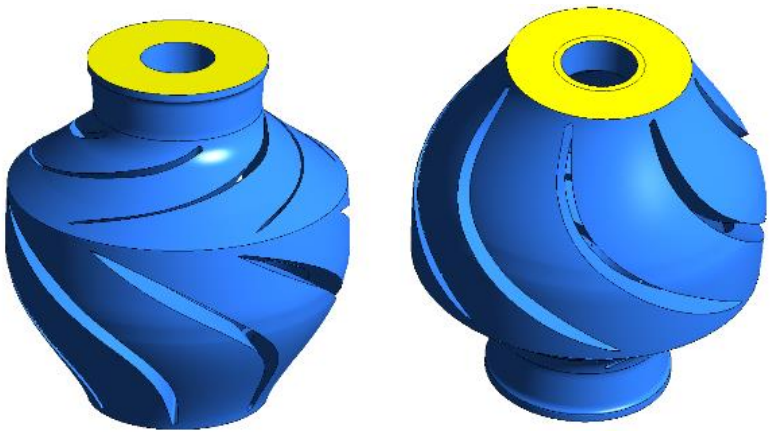

Figure VI-1. Location of surfaces for inlet pressure i.e. at stage inlet (left) and outlet pressure i.e. at diffuser outlet (right) calculation to obtain the pressure rise as a result of energy input in the pump.

Since the value of 100 psi has been imposed on the outlet, only the stage inlet pressure was calculated by considering the area averaged value of pressure (Fig. VI-1). Therefore the difference was calculated as $P_{out} - P_{in} = \Delta P =$ pressure rise of the stage.

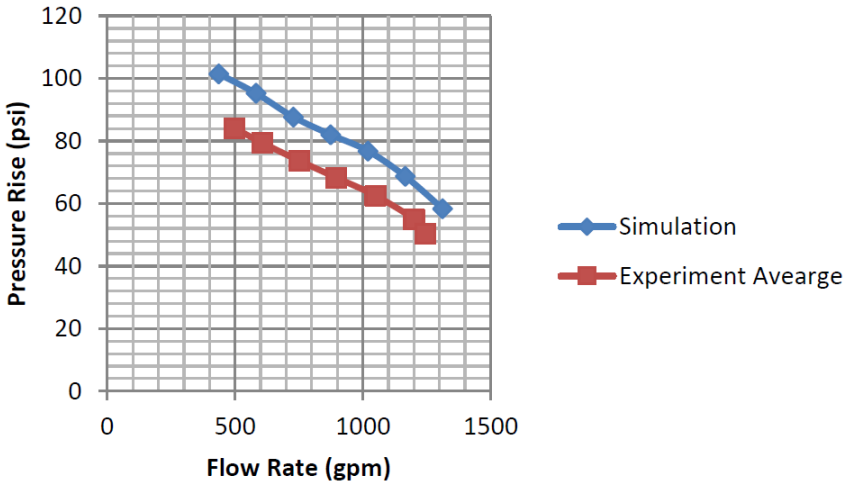

Figure VI-2. The comparison of numerical data with the experimental data for pure water. [12]

Using this definition, Yin [12] concluded that simulation results yielded a higher value of pressure rise through the stage as compared to the experimental data (Fig. VI-2). This is reasonable as secondary leakages through seals and balance holes were neglected. He also concluded that on reducing the pressure rise obtained from CFD analysis by 14 psi, good agreement with the experimental data was obtained. Therefore, it can be stated that there is a consistent increase in pressure rise owing to our simplifying assumptions, which indirectly provides an idea of the extent of head that we have gained by not including balance holes, flow leakages, secondary flow, etc. This also validates our model of CFD analysis of WJE-1000 electrical submersible pump.

6.2 Flow Analysis

The flow field in pump's main hydraulic paths was analyzed in CFD-Post software. Four different cases are selected to study the influence of flow rate, viscosity,

and speed on the streamlines or nature of the flow. Yin [12] performed a similar analysis at 3600 rpm, therefore, to avoid the redundancy, this analysis focuses on 3000 rpm (three cases) and at 4200 rpm (one case), thereby covering all the input parameters.

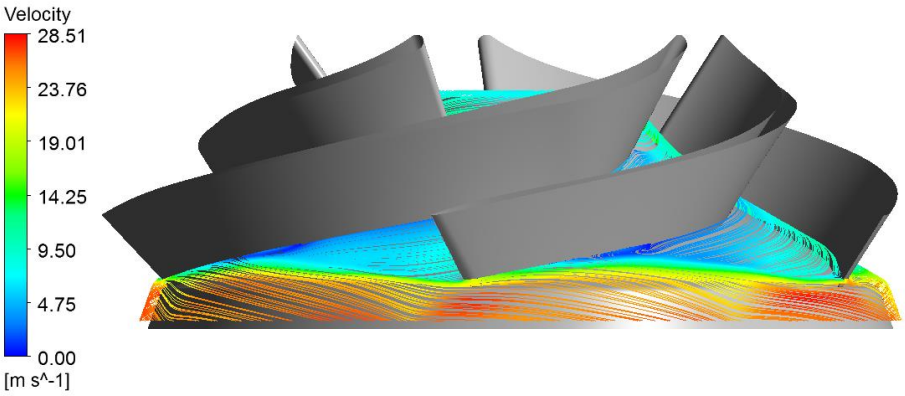

Figure VI-3 Streamlines in impeller for 2.4 cP 3000 rpm 444.7 gpm case.

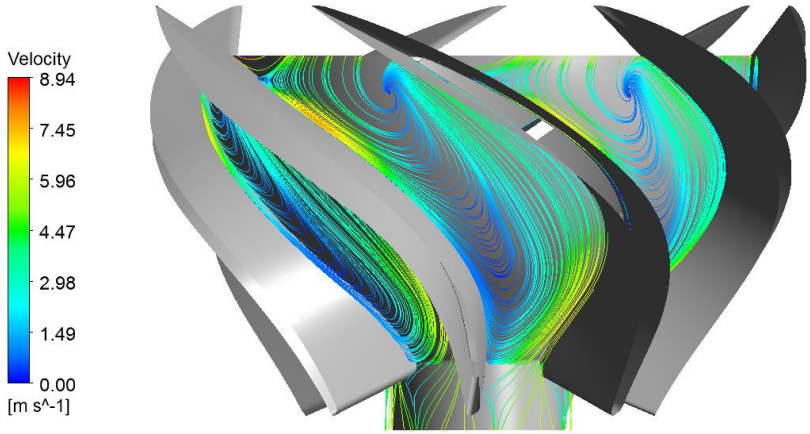

Figure VI-4 Streamlines in diffuser for 2.4 cP-3000 rpm 444.7 gpm case.

Figure VI-3 and VI-4 show the streamlines for a pump speed of 3000 rpm using 2.4 cP oil at 444.7 gpm (low flow rate, low viscosity and lower rpm case) for the impeller and diffuser respectively. It can be seen that large and numerous recirculation zones are present in the diffuser.

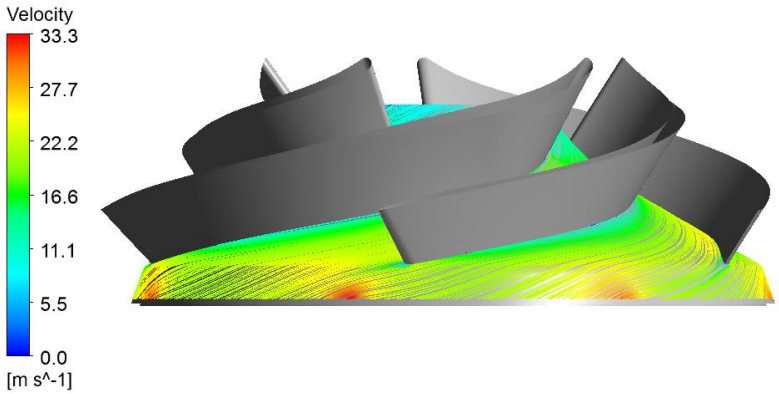

Figure VI-5 Streamlines in impeller for 2.4 cP-3000 rpm 1334.09 gpm case.

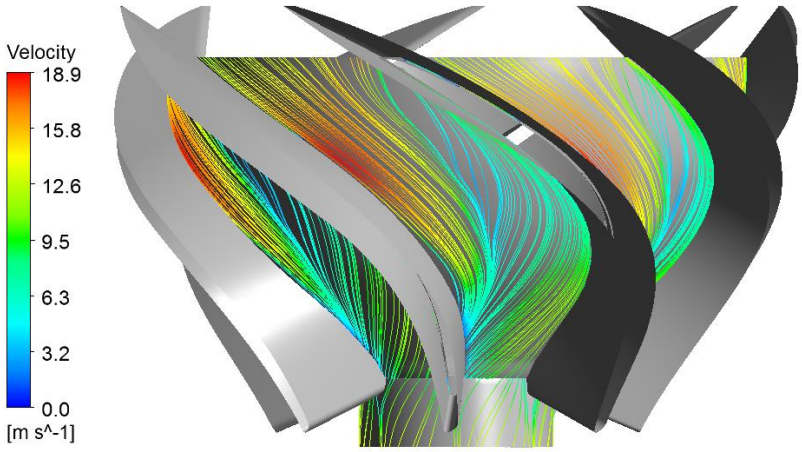

Figure VI-6 Streamlines in diffuser for 2.4 cP-3000 rpm 1334.09 gpm case.

However, in figures VI-5 and VI-6 for the same speed and fluid but a higher flow rate (1334.09 gpm), (lower speed, low viscosity and high flow rate) case, the recirculation zones are smaller and fewer in number as compared to the low flow rate case (Fig. VI-3, VI-4). A higher flow rate indeed leads to a smoother flow behavior.

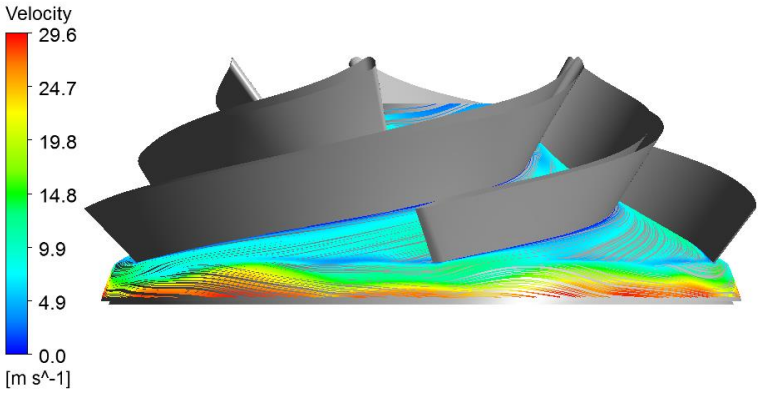

Figure VI-7 Streamlines in impeller for 400 cP-3000 rpm 444.7 gpm case.

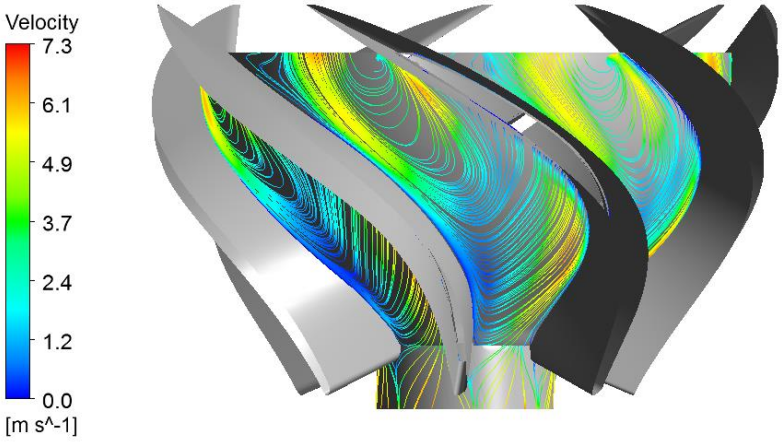

Figure VI-8 Streamlines in diffuser for 400 cP-3000 rpm 444.7 gpm case.

Figures VI-7, VI-8, show the streamlines for a lower rpm, low flow rate and high viscosity case (3000 rpm, 444.7 gpm, 400 cP) for the impeller and diffuser respectively. It can be seen that the recirculation zones are fewer and smaller as compared to a low viscosity case (owing to increased viscous nature of the flow). However the amount of recirculation is certainly more than for the low viscosity and higher flow rate case.

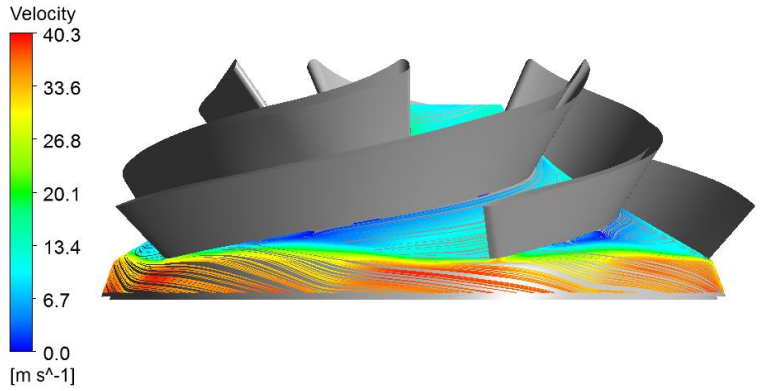

Figure VI-9 Streamlines in impeller for 2.4 cP-4200 rpm 622.58 gpm case.

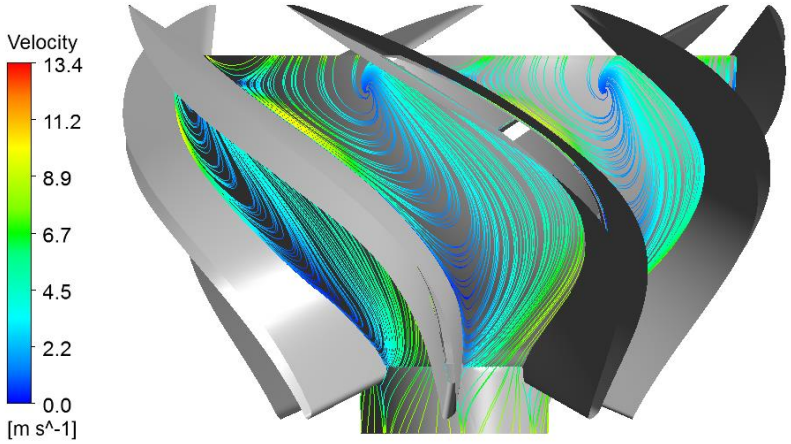

Figure VI-10 Streamlines in diffuser for 2.4 cP-4200 rpm 622.58 gpm case.

Figures VI-9, VI-10 show the streamlines for a higher speed, low flow rate and low viscosity case (4200 rpm, 622.58 gpm, 2.4cP). It is quite similar to the figures VI-3, VI-4, indicating that there is no significant difference in the flow behavior with a change in rotational speed of the pump.

A comparison with Yin's [12] analysis establishes that the flow behavior does not change significantly with a change in rotational speed, however the change in behavior is quite consistent with changing viscosity and flow rate at different rotational speeds.

6.3. Performance Analysis

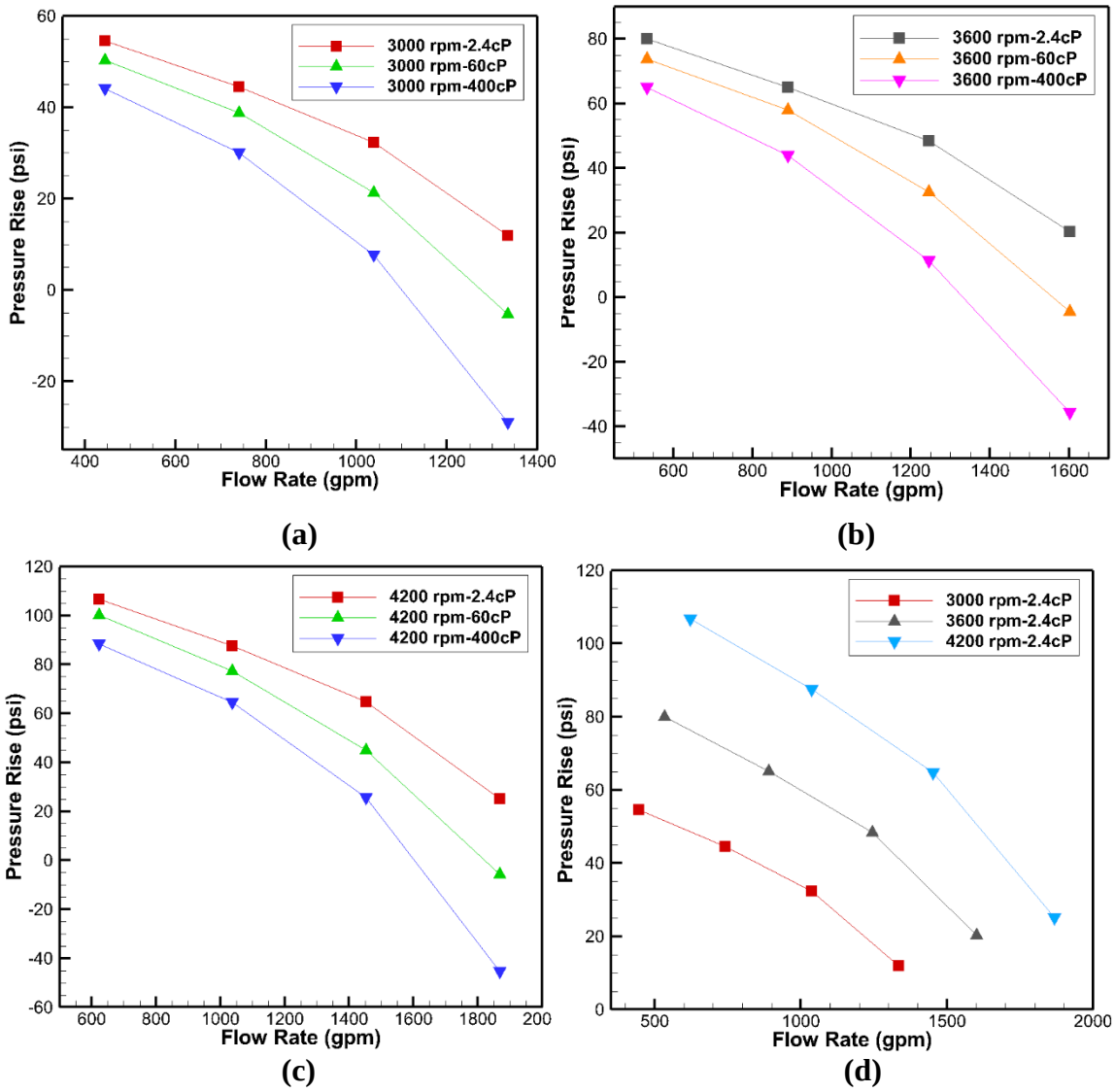

Figure VI-11 Variation in pressure rise through stage of the pump with flow rate at 3000 rpm (a), 3600 rpm (b), 4200 rpm (c) and for 2.4cP oil with different rotational speeds (d).

Figures (VI-11) show that for different rotational speeds of the pump, there is a common trend in the variation of ΔP with Q, i.e. with an increase in viscosity, the pressure rise decreases, the reason being, more of the input energy is used to overcome friction losses. Therefore, a lesser fraction of the input power is converted into head. Also, for a few cases the pressure rise is negative. The reason lies in the fact that the operating conditions for those cases (i.e. combination of flow rate, viscosity and rotational speed) are beyond the capacity of the pump, therefore it is observed that in order to overcome the losses, even greater amount of energy input is required. Therefore, these points are unrealistic but have been included here only for the sake of completeness and illustrating that there is indeed a point beyond which the pump is inoperable.

Now, let us consider the definition of hydraulic efficiency or simply efficiency. The expression for efficiency is given as:

$$\eta = \frac{\rho g Q H}{T\omega} = \frac{\mathcal{P}_{out}}{\mathcal{P}_{in}} \tag{VI-1}$$

where, ρ is the density of fluid in kg/m^3, $g = 9.8\ m/s^2$ is the gravitational acceleration, Q is the flow rate in m^3/s, H is the head generated by the pump in m, T is the torque on the shaft in $N-m$ due to power input, ω is the rotational speed of the pump in rad/s, $\mathcal{P}_{out}$ is the power output realized by the head or pressure difference generated by the pump, $\mathcal{P}_{in}$ is the power input to the system in the form of electrical energy.

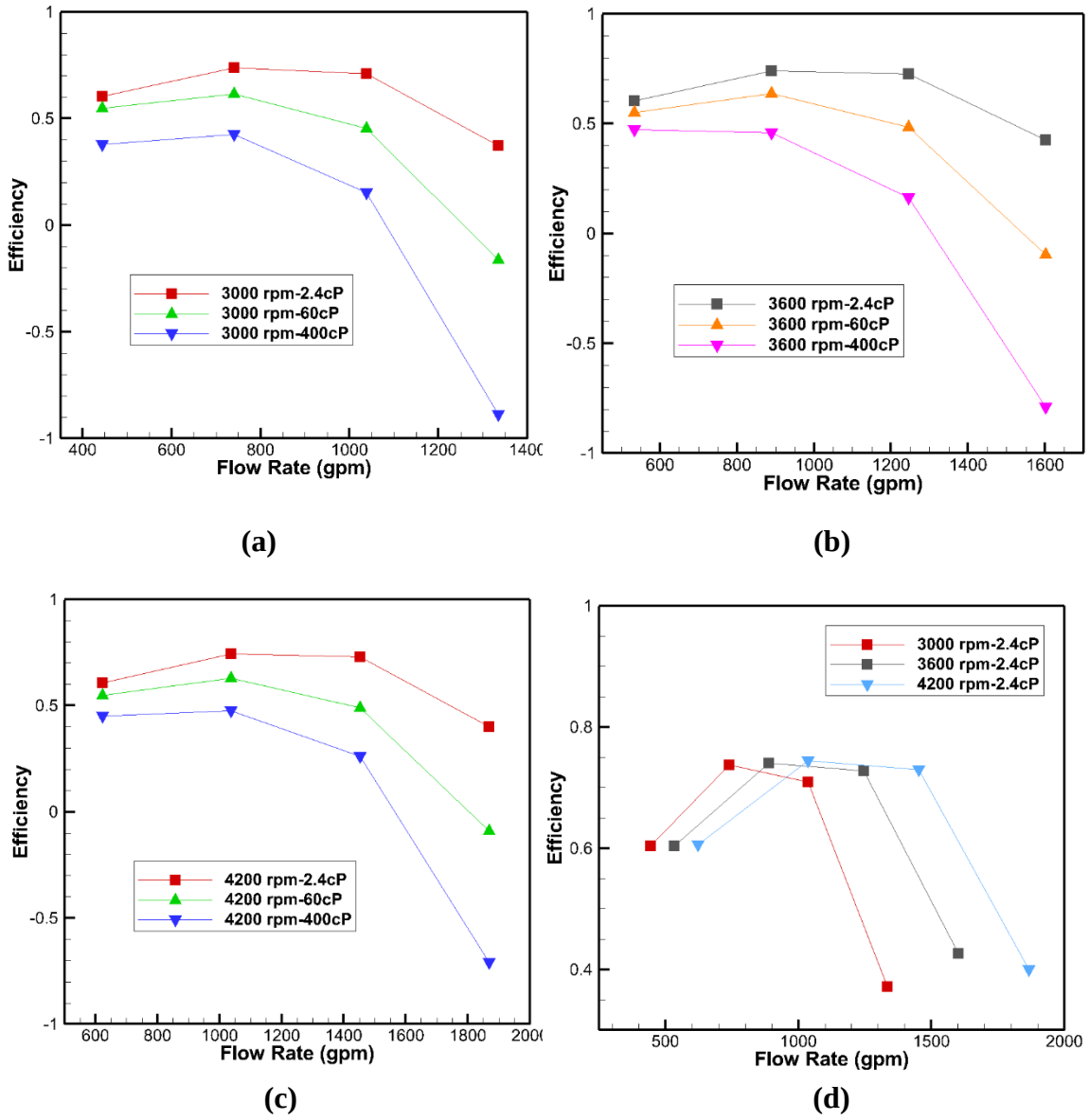

Figure VI-12. Variation of efficiency of the stage of the pump with flow rate at 3000 rpm (a), 3600 rpm (b), 4200 rpm (c) and for 2.4cP oil with different rotational speeds (d).

From the figures above (VI-12) it is illustrated that the hydraulic efficiency of the pump for a particular fluid, first increases to a maximum value (this point is also known

as the best efficiency point or simply BEP) and then gradually decreases. This is common across all viscosities and rotational speeds. There are some cases for which the hydraulic efficiency is negative, this simply means that in a practical case, this set of operating conditions is not applicable for this particular pump but has been included here only for the sake of completeness. Another observation that can be made here is that the efficiency decreases with an increase in viscosity of the fluid at any rotational speed. This can be directly correlated to the fact that a more viscous fluid results in greater frictional losses. Therefore, the pump converts a lesser fraction of input energy to the desired output, in this case the pressure rise or the head.

An observation here (VI-12-(d)) is that for a particular fluid, at a fixed flow rate, efficiency decreases with increasing rotational speed of the pump, for low flow rates till the BEP. However, this behavior reverses as the BEP is crossed on the horizontal axis. Also, at different rotational speeds, the pump has different values of BEP. The flow rate at which highest efficiency is attained, increases with an increase in the rotational speed of the pump but, the highest efficiency that could be attained remains the same.

6.4. Dimensionless Analysis

Dimensionless analysis forms an important part of this study, as it allows analysis of the data with an objectivity that focuses on a few dimensionless numbers, coefficients, and ratios, instead of all the cumbersome details of the setup and also helps us to work across the combinations of geometries and operating conditions. The standard affinity law numbers are considered along with others in an attempt at establishing a modification of

the similarity laws for centrifugal pumps to include working at different rotational speeds, viscosities and flow rates:

$$\psi = \frac{\Delta P}{\rho D_s^2 \omega^2} \tag{VI-2}$$

$$\phi = \frac{Q}{\omega D_s^3} \tag{VI-3}$$

$$Re_w = \frac{\rho \omega D_s^2}{\mu} \tag{VI-4}$$

$$N_{sh} = \frac{\mathcal{P}_{sh}}{\rho D_s^5 \omega^3} \tag{VI-5}$$

$$N_{out} = \frac{\rho Q g H}{\rho D_s^5 \omega^3} \tag{VI-6}$$

$$N_{drag} = \frac{\mathcal{P}_{drag}}{\rho D_s^5 \omega^3} \tag{VI-7}$$

$$\mathcal{P}_{drag} = \mathcal{P}_{sh} - \rho Q g H \tag{VI-8}$$

where, ψ is the head coefficient, ΔP is the pressure rise through the pump in $Pascals\ or\ Nm^{-2}$, ρ is the density of the fluid in kg/m^3, $D_s = 200.8\,mm$, is the length scale (diameter) of pump geometries, ω is the rotational speed of the pump in rad/s, ϕ is the flow coefficient, Q is the flow rate in m^3/s, Re_w is the rotational Reynold's number, μ is the dynamic viscosity of the fluid in $Pa - s$ or $kgm^{-1}s^{-1}$, N_{sh} is the shaft power coefficient, $\mathcal{P}_{sh}$, is the shaft power in Watts or Nms^{-1}, N_{out} is the output power coefficient, $g = 9.8\,m/s^2$ is the acceleration due to gravity, H is the head generated by the pump in meters, N_{drag} is the drag power coefficient and $\mathcal{P}_{drag}$ is the drag power generated due to various kinds of losses in Watts or Nms^{-1}.

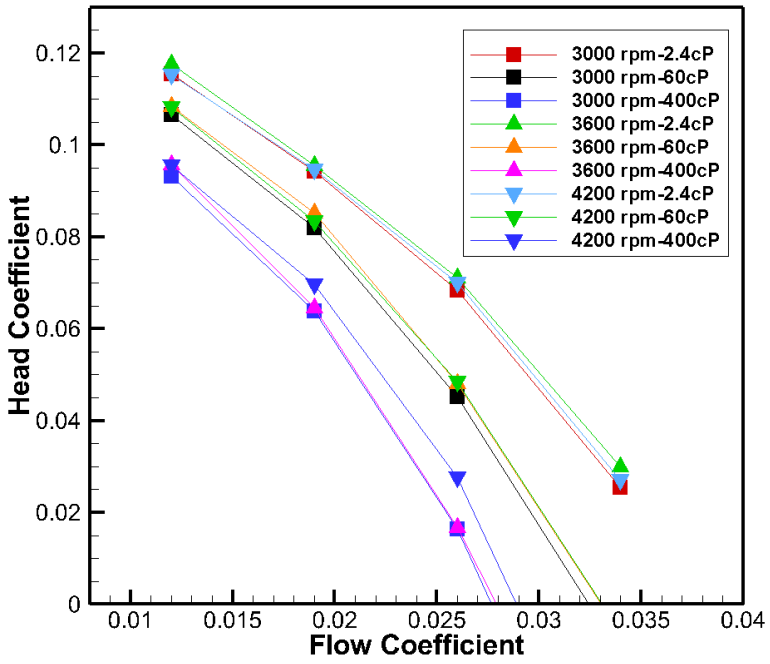

Figure VI-13 Variation of head coefficient with flow coefficient for different viscosities and rotational speeds.

In Figure VI-13, the cases with $Re_{Dh} < 2300$, have been simulated using the laminar flow model. It is very clear that for a particular viscosity, the head coefficient does not vary with rotational speed as the data for 2.4cP coincide for different rpm. Similarly, data for 60cP coincide for different rpm. However, it might appear that there is a discrepancy in the case of 400cP data where not all the points for different rpm coincide. This apparent discrepancy is due to our selection of simulation model (laminar or turbulent) based on hydraulic Reynold's number (Re_{Dh}). In reality there is no sharp boundary between laminar and turbulent as there is also a transition flow regime that exists. So, a better selection of simulation model for Re_{Dh} close to 2300 might fix this apparent discrepancy. This is discussed further in the section laminar vs turbulent

modeling. The standard affinity laws are obeyed for each viscosity, that is head coefficient is only a function of flow coefficient. However, the effect of viscosity is clearly demonstrated by each viscosity having a different curve.

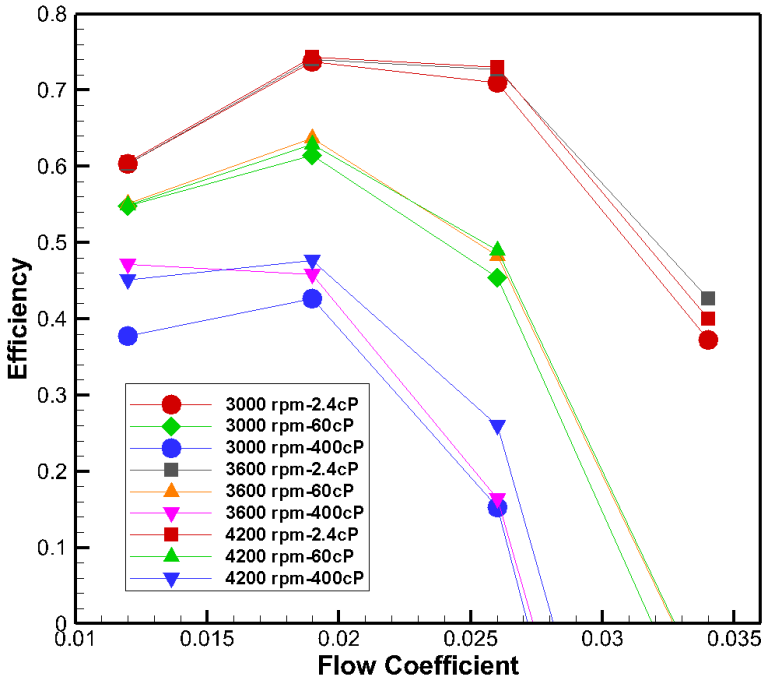

Figure VI-14. Variation of hydraulic efficiency with the flow coefficient.

The efficiency curves for various viscosities (Figure VI-14) show that the rotational speed of the pump does not make a significant difference. It can be noted from here that, however, for highly viscous cases, i.e. 400cP, there is some discrepancy in efficiency with changing rpm of the pump. We can attribute this to the choice of model for simulation. If we take a look at these cases, the hydraulic Reynold's number for 400cP cases are either very low or ~ 2300. Therefore, fine-tuning of the simulation model for

such cases is required to get an even better agreement. These data show the same effect of viscosity upon the affinity law curve. For a constant viscosity, a single curve represents efficiency as a function of flow coefficient (pump speed and flow rate) as was observed for the head coefficient.

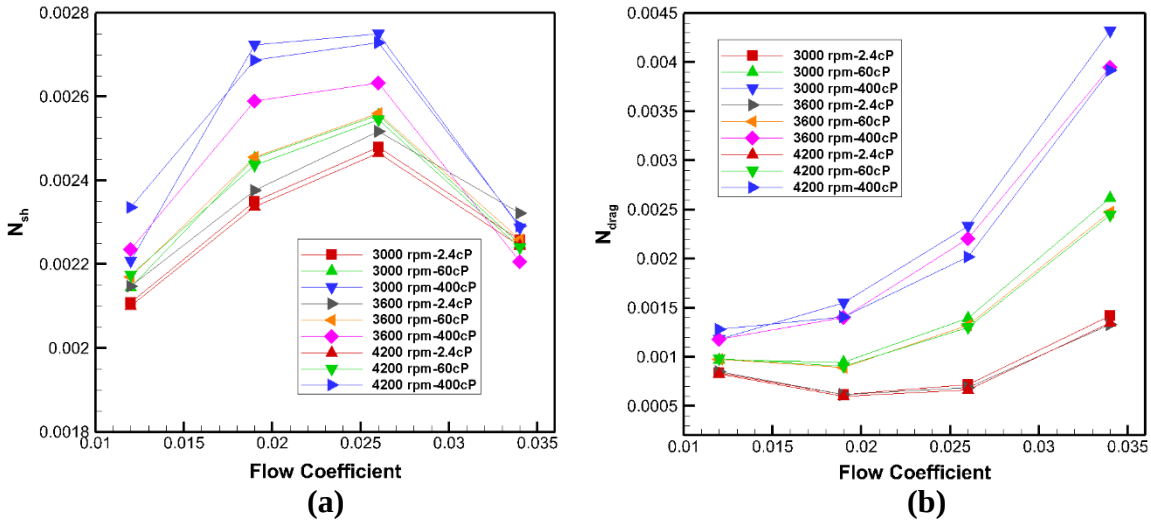

Figure VI-15. Variation of shaft power coefficient (a) and drag power coefficient (b) with flow coefficient.

From VI-15 (a), it can be observed that shaft power increases with an increase in viscosity of the fluid. It can be explained as a greater power input is required to move a fluid of greater viscosity as a greater resistance is offered by the more viscous fluid.

From VI-15 (b) it can be noted that increasing viscosity and at higher flow rates, drag power increases due to an increase in viscous losses. Rotational speed of the pump does not have a significant effect on the drag coefficient, it is similar for different rotational speeds if the flow coefficient is unchanged.

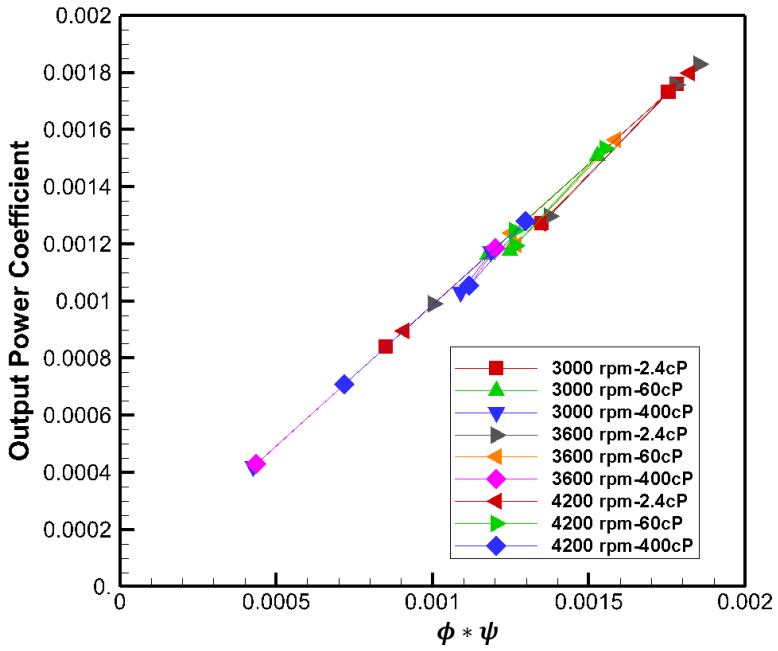

Figure VI-16. Variation of output power coefficient N_{out} with the product of flow rate coefficient and head coefficient $\phi * \psi$.

Figure VI-16 verifies that the output power coefficient (hydraulic power added to the fluid) is equal to the flow coefficient times the head coefficient. This nature of the plot $y = x$ line or $N_{out} = \phi * \psi$ line perfectly makes sense as according to the definitions of these dimensionless numbers it should hold theoretically. This further verifies our simulation methodology and further strengthens our claims regarding the plot of interdependence of efficiency, flow coefficient and rotating Reynold's number. These data show how viscosity affects the affinity laws. The goal is to modify the affinity laws to obtain one non-dimensional head-flow rate curve and one efficiency curve for all viscosities.

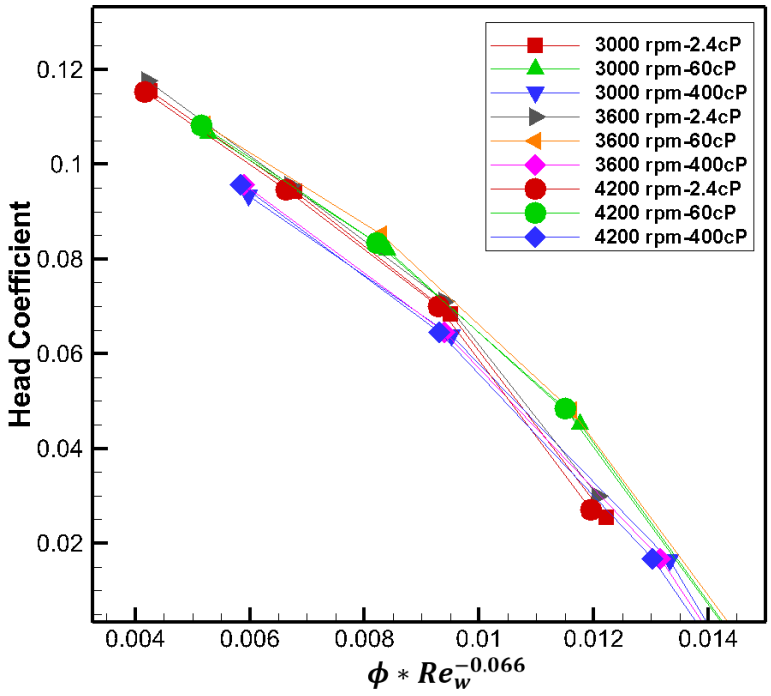

Figure VI-17.Variation of head coefficient ψ, with flow coefficient ϕ and rotating Reynold's number Re_w.

The effects of viscosity are to be included using the rotational Reynold's number, Re_w. It was discovered that by multiplying the flow coefficient by the rotational Reynold's number raised to a power (similar to pipe flow friction factor having a similar relationship) results in a single head coefficient curve which includes the effects of viscosity. The horizontal axis represents $\phi * Re_w^{-0.066}$ i.e. product of flow coefficient and rotating Reynold's number raised to index -0.066. This interdependence was identified by Yin [12] and this study supports that interdependence as it is clear that even for different rotational speeds of the pump, or in general different sets of operating conditions, data points fall on the same plot (Figure VI-17).

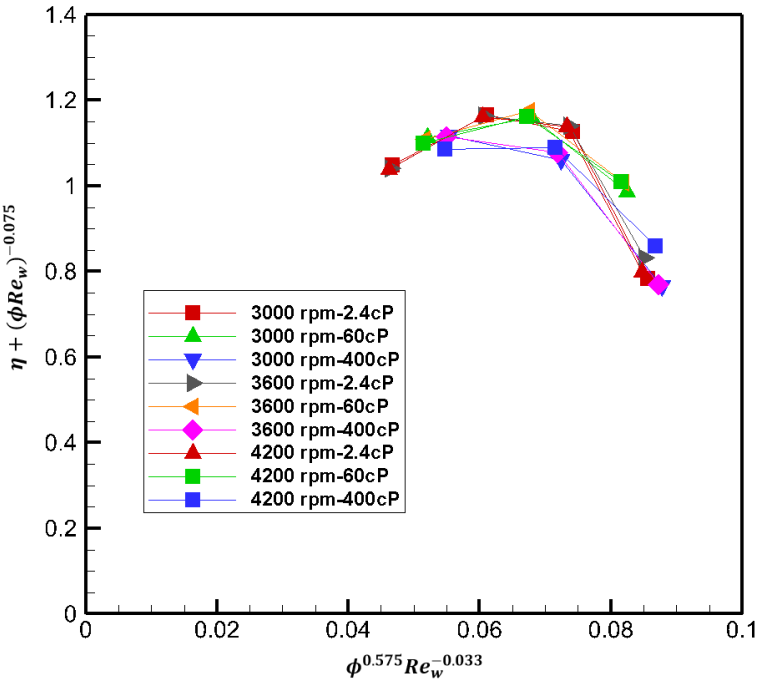

Figure VI-18. Dependence of efficiency on flow coefficient ϕ and rotating Reynold's number Re_w (a).The vertical axis (ordinate) represents $\eta + (\phi * Re_w)^{-0.075}$ and the horizontal axis (abscissa) represents $\phi^{0.575} Re_w^{-0.033}$.

Further analysis of the pump efficiency dependence upon Re_w results in Figure VI-18 which indicates that it is indeed possible to predict the efficiency of a pump, for the ESP WJE-1000, for a given set of operating conditions. This plot represents the data that covers a wide range of operating conditions and the points falling within these bounds can be interpolated by knowing the equation of the curve or by simply locating the point on the curve itself.

To lend more credibility to this proposition, all the data generated by Yin [12] and that was generated in this study were compiled and plotted for the same horizontal and vertical axes. The plot is shown below.

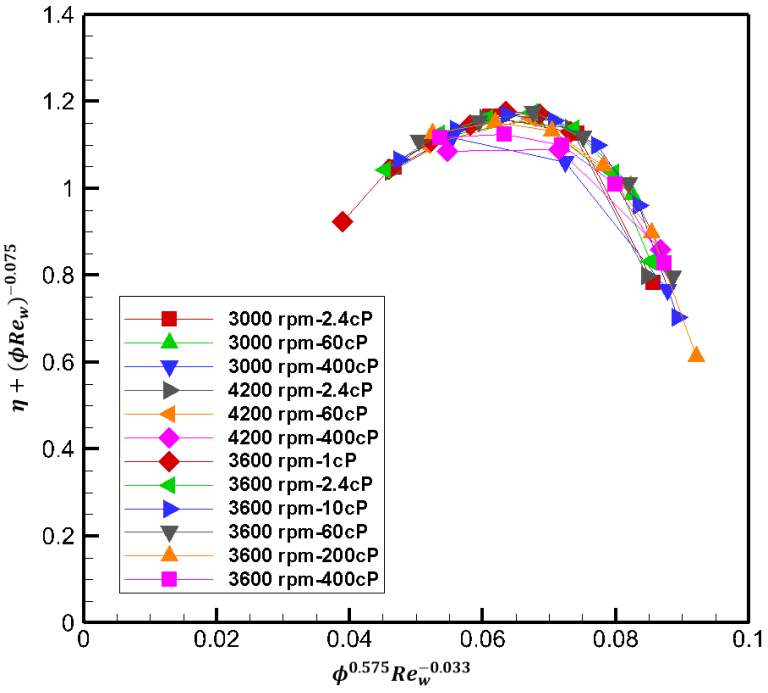

Figure VI-19. Dependence of efficiency on flow coefficient ϕ and rotating Reynold's number Re_w (b). The vertical axis (ordinate) represents $\eta + (\phi * Re_w)^{-0.075}$ and the horizontal axis (abscissa) represents $\phi^{0.575} Re_w^{-0.033}$.

This (Fig. VI-19) indeed shows that for a wide range of operating conditions, one can reasonably predict the efficiency, given the flow coefficient and rotating Reynold's number.

A closer look at the plot also indicates that it might be possible to group the data for laminar and turbulent flow cases separately, or in other words, it is possible to have two different such curves for a pump based on Re_{Dh}, that gives an idea of the nature of the flow and categorizing it into either laminar or turbulent regime. A further analysis showed that neither of the two gave significant improvement on these results, and one might need to look at the transition flow models in the Fluent software [13], and apply them accordingly. This arises from the fact that there is no established number based on which to categorize the flow perfectly into laminar or turbulent or transition regime. Therefore, further study is required.

The ramifications of these results are very significant. The affinity laws have been modified to include the effects of viscosity. Hence a single head coefficient curve and a single efficiency curve (power required to operate the pump) can represent the pump performance over the entire flow rate and pump speed envelop. This will allow operators to be able to predict changes in pump performance with varying fluids and pump speeds. An additional benefit is that a pump need not be tested over a wide range of fluids, but only at two viscosities in order to obtain power law coefficient on Re_w. Once the relationship has been determined for a specific pump design, it can be published and utilized for all operating conditions.

6.5 Laminar vs Turbulent Modeling

In this study, as previously mentioned, cases with hydraulic Reynolds number less than 2300 i.e. $Re_{Dh} < 2300$ were simulated using the laminar model (Table VI-1). Although it was expected that this should be in sync with our general understanding of categorizing a flow regime as being either laminar or turbulent and thus give expected results, i.e. follow the trends as applicable for high Reynold's number cases which are clearly turbulent. But the results indicated that this assumption was rather less satisfactory. The laminar cases were then simulated using exactly the same model as turbulent cases. The results are presented in the figures to follow.

Table VI-1 Cases simulated using laminar model

Viscosity (cP)	RPM	Flow Rate (gpm)	Re_{Dh}	Nature
400	3000	444.7	443.659	Laminar
400	3000	741.06	739.316	Laminar
400	3000	1037.63	1035.189	Laminar
400	4200	622.58	621.122	Laminar
400	4200	1037.48	1035.043	Laminar
400	4200	1452.68	1449.264	Laminar

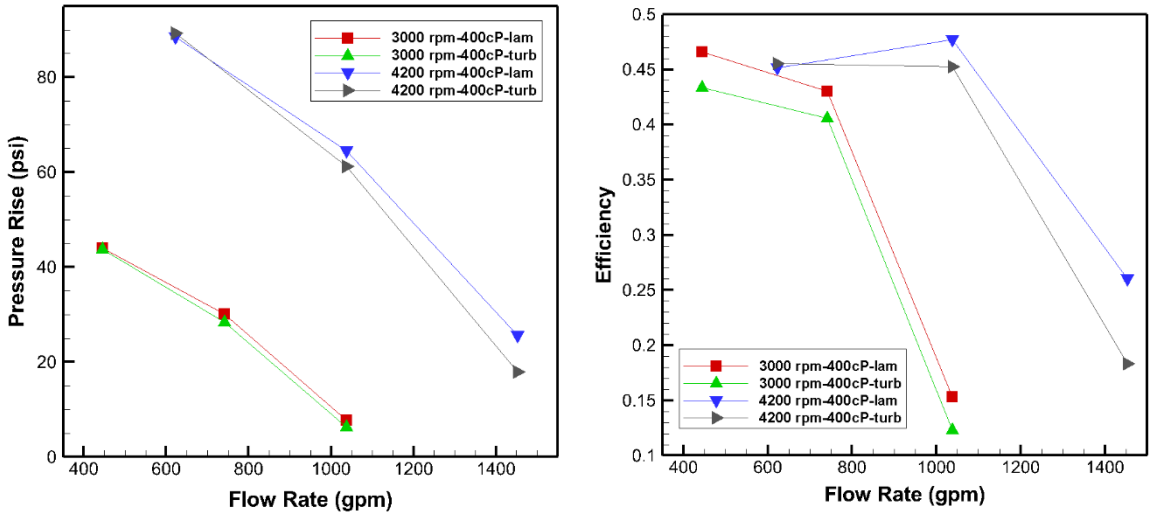

Figure VI-20. Variation of pressure rise (a) and efficiency (b) with flow rate for 400cp cases considering both laminar and turbulent models at 3000 rpm and 4200 rpm.

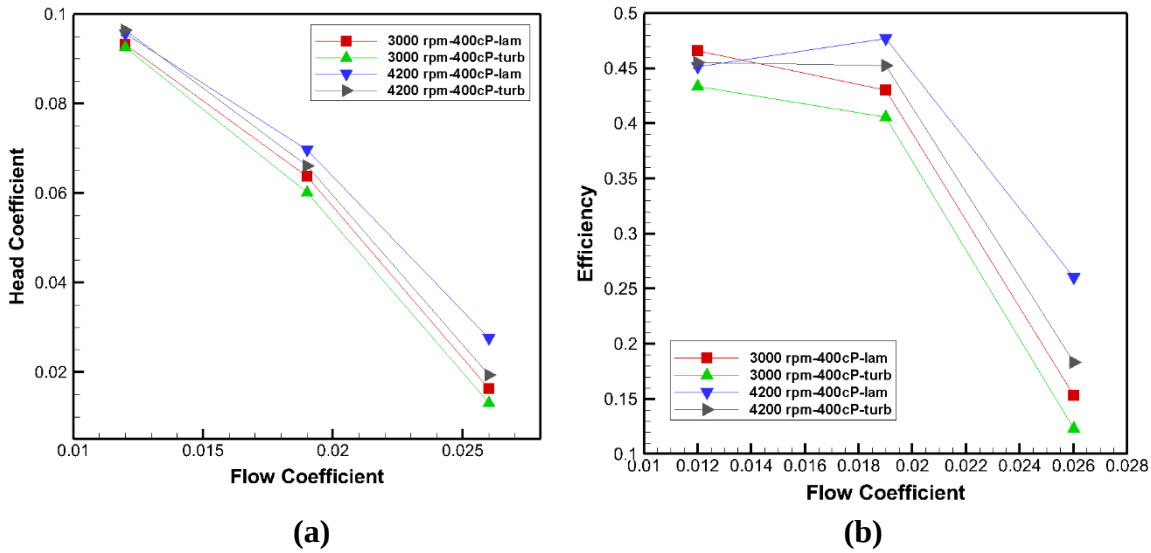

Figure VI-21. Variation of head coefficient ψ (a) and efficiency (b) with flow coefficient ϕ for 400cp cases considering both laminar and turbulent models at 3000 rpm and 4200 rpm.

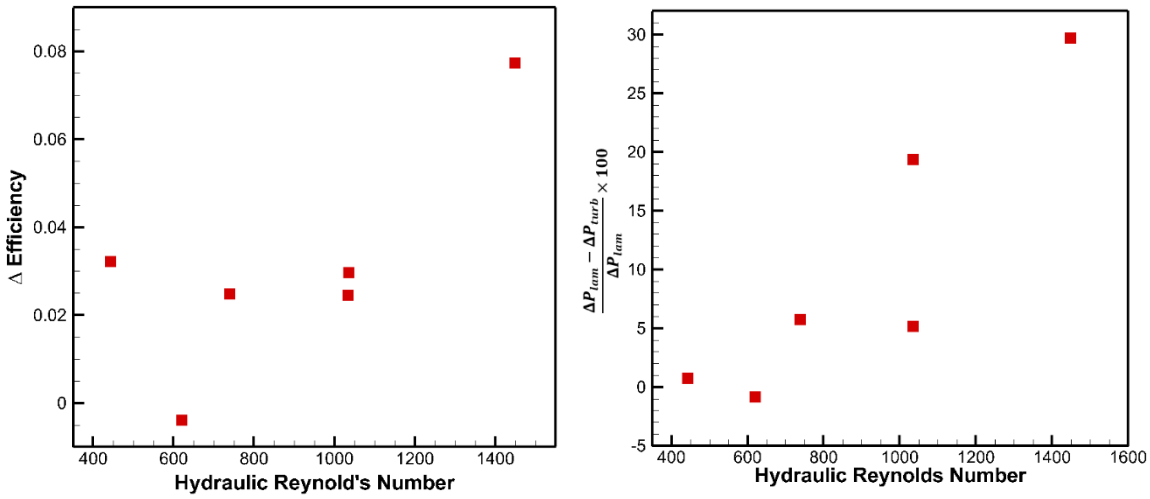

(a) **(b)**

Figure VI-22. Variation of difference between efficiencies of laminar and turbulent models $\eta_{laminar} - \eta_{turbulent}$ (a) and % change in the relative pressure rise of the two models $\frac{\Delta P_{lam} - \Delta P_{turb}}{\Delta P_{lam}} \times 100$ (b) for 400cP 3000 rpm and 4200 rpm cases with hydraulic Reynold's number Re_{Dh} as defined earlier.

From the figures above (Fig. VI-20, VI-21, VI-22), it is clear that there indeed is a difference in pressure rise, efficiencies, and head coefficient, depending on our choice of the simulation model. However, the difference is significant only towards the higher Re_{Dh} side. Although for Reynold's number lower than 1000, the difference between the results based on the two simulation models is not significant, the choice of laminar model over turbulent model indeed gives a higher pressure rise, and a higher efficiency, and it is more in sync with the non-dimensionalized parameters and their curves that we have considered. However, as we consider Reynold's number greater than 1000 but still lower than 2300 i.e.$1000 < Re_{Dh} < 2300$, the difference between the results obtained from two models

increases. The discrepancy increases in a particular range of Re_{Dh}. It could very well be the transition regime and therefore needs to be studied more carefully with more sophisticated models. Therefore, we conclude that laminar model works well for low Reynold's numbers or $Re_{Dh} < 1000$ but neither laminar nor turbulent model works well for $1000 < Re_{Dh} < 2300$. Since, in our study, the number for deciding the flow regime as laminar or turbulent was set at 2300 based on established literature, we can either continue with this same number 2300 or pursue obtaining extensive simulations/experimental data to help establish some other number or a range as well. However, for the time being it is safe to categorize the flow regimes as the following:

$Re_{Dh} < 1000$	Laminar
$1000 < Re_{Dh} < 2300$	Transition
$Re_{Dh} > 2300$	Turbulent

7. CONCLUSIONS

From this study, the following conclusions can be drawn:

1) The pressure difference through the stage of the pump increases with an increase in rotational speed, keeping the viscosity and flow rate the same.

2) The pressure difference and hydraulic efficiency through the stage of the pump decreases with an increase in viscosity keeping the flow rate and rotational speed the same.

3) For the same flow coefficient and viscosity, efficiency and the head coefficient does not change with rotational speed of the shaft.

4) For WJE-1000, the head coefficient data for different rotational speeds, also fall on the same curve as proposed by Yin [12] i.e. $\psi \; vs \; \phi * Re_w^{-0.066}$.

5) For WJE-1000, the efficiency data for different rotational speeds, viscosities, flow rates can be represented on a single curve on the plot of $\eta + (\phi * Re_w)^{-0.075} \; vs \; \phi^{0.575} * Re_w^{-0.033}$.

6) The ramifications of these results are very significant. The affinity laws have been modified to include the effects of viscosity. Hence a single head coefficient curve and a single efficiency curve (power required to operate the pump) can represent the pump performance over the entire flow rated and pump speed envelop. This will allow operators to be able to predict changes in pump performance with varying fluids and pump speeds. An additional benefit is that a pump need not be tested over a wide range of fluids, but only at two viscosities in order to obtain

power law coefficient on Re_w. Once the relationship has been determined for a specific pump design, it can be published and utilized for all operating conditions.

REFERENCES

1. Karassik, I. And J.T. mcguire, *Centrifugal pumps*. 2012: Springer Science & Business Media.
2. Ippen, A.T., *The influence of viscosity on centrifugal pump performance*. 1945: American Society of Mechanical Engineers.
3. Gülich, J., *Pumping highly viscous fluids with centrifugal pumps—Part 1.* World Pumps, 1999. **1999**(395): p. 30-34.
4. Gülich, J., *Pumping highly viscous fluids with centrifugal pumps—Part 2.* World Pumps, 1999. **1999**(396): p. 39-42.
5. Timar, P., *Dimensionless characteristics of centrifugal pump.* Chemical Papers-Slovak Academy of Sciences, 2005. **59**(6B): p. 500.
6. Feng, J., F.-K. Benra, and H. Dohmen, *Application of different turbulence models in unsteady flow simulations of a radial diffuser pump.* Forschung im Ingenieurwesen, 2010. **74**(3): p. 123-133.
7. Majidi, K. and H. Siekmann, *Numerical calculation of secondary flow in pump volute and circular casings using 3D viscous flow techniques.* International Journal of Rotating Machinery, 2000. **6**(4): p. 245-252.
8. Barrios, L.J., *Visualization and modeling of multiphase performance inside an electrical submersible pump*. 2007: (PhD. Dissertation, The University of Tulsa, Petroleum Engineering Department, Tulsa, OK).
9. Sun, D. and M.G. Prado, *Single-phase model for electric submersible pump (ESP) head performance.* SPE Journal, 2006. **11**(01): p. 80-88.

10. Sirino, T., H. Stel, and R.E. Morales. *Numerical study of the influence of viscosity on the performance of an electrical submersible pump*. in ASME 2013 Fluids Engineering Division Summer Meeting. 2013. American Society of Mechanical Engineers.

11. Stel, H., et al. *CFD investigation of the effect of viscosity on a three-stage electric submersible pump*. in ASME 2014 4th Joint US-European Fluids Engineering Division Summer Meeting Collocated With the ASME 2014 12th International Conference on Nanochannels, Microchannels, and Minichannels. 2014. American Society of Mechanical Engineers.

12. Yin, W., *CFD simulation of the influence of viscosity on an electrical submersible pump,* in *Mechanical Engineering*. 2016: (MS Thesis, Mechanical Engineering Department, Texas A&M College Station).

13. Fluent, A., *Ansys fluent theory guide.* ANSYS Inc., USA, 2011.

14. Bellevue, W., *Tecplot user's manual.* Amtec Engineering Inc, 2003.

15. Carvajal Diaz, N., *Effects of sand on the components and performance of electric submersible pumps*. 2012: (MS Thesis, Mechanical Engineering Department, Texas A&M College Station).

16. *Conosol Products*. 2008, Calumet Speciaty Products Parteners, L.P.